Numerical model for the determination of the reduced electric field in a CO_2 microwave plasma derived by the principle of impedance matching

P.W.C. Groen[1], A.J. Wolf[1], T.W.H. Righart[1], M.C.M. van de Sanden[1,2], F.J.J. Peeters[1], and W.A. Bongers[1]

[1]DIFFER - Dutch Institute For Fundamental Energy Research, De Zaale 20, 5612 AJ Eindhoven, the Netherlands
[2]Department of Applied Physics, Eindhoven University of Technology, PO Box 513, 5600 MB Eindhoven, the Netherlands

Abstract

Three dimensional electromagnetic modelling of a free-standing CO_2 microwave plasma has been performed, by describing the plasma as a dielectric medium. The relative permittivity and conductivity of the medium are parametrised. The waveguide geometry from experiment, including the tuner, is put into the model, knowing that this corresponds to maximum power transfer of the microwave generator to the plasma under plasma impedance matching conditions. Two CO_2 plasma discharge regimes, differing mainly in pressure, input power and temperature, have been studied. The model's validity has been checked through study of materials of known conductivity. From measurements of the neutral gas temperature and the plasma electron density profile, the reduced electric field is determined. From the parametrisation of the dielectric properties, a range for the effective electron-neutral collision frequency for momentum transfer is estimated. The results for the reduced electric field and the range of the electron neutral collision frequency obtained, are consistent as verified by simulations using BOLSIG+. In addition, from this comparison it

is possible to narrow down the range of the collision frequencies, and to estimate the electron temperature. The reduced electric field lies between 80 and 180 Td for the relatively low pressure, low input power, the so-called 'diffuse' regime. For the relatively high pressure, high input power ('contracted') regime it lies between 10 and 60 Td. The normalised collision frequency lies between 1.6 and 2.3 for the diffuse regime, while for the contracted regime it lies between 2 and 3. The electron temperature ranges from 2 to 3 eV for the diffuse regime, and from 0.5 to 1 eV for the contracted regime.

1 Introduction

In the field of CO_2 utilisation, a topic of interest is the dissociation of CO_2 molecules using a microwave plasma, with the ultimate aim of producing synthetic fuels [1, 2]. For this goal it is essential to dissociate the molecules in an energy efficient way. This demands optimizing the microwave plasma to obtain optimal plasma parameter values, such as electron density (n_e), electron-neutral collision frequency for momentum transfer (ν, from here on referred to as just the 'collision frequency') and electron temperature (T_e). These plasma parameters can be conveniently captured using the single scaling parameter of reduced electric field E/n_0, where E is the electric field experienced by free electrons in the plasma and n_0 is the neutral gas density. The reduced electric field is crucial in tuning the electron energy distribution to primarily excite the asymmetric vibrational stretching mode in CO_2 molecule, where values of $E/n_0 = 20$ Td ($= 2 \times 10^{-20}$ V m^2) are expected to lead to high energy efficiencies for CO_2 dissociation via a 'vibrational ladder climbing' process [3].

The aim of this work is to derive plasma parameters, such as E/n_0, of microwave plasma using the principle of impedance matching. In the experimental microwave plasma reactor, a free-standing plasma is ignited inside a quartz tube perpendicularly crossing the waveguide. To optimize the power transfer between microwave source and plasma, the waveguide is physically tuned using movable metal stubs, so that the effective impedance Z_{in} for microwaves propagating towards the plasma matches the characteristic (wave) impedance of the waveguide Z_0. In this way, the reflection coefficient for microwaves at the input port of the tuner + waveguide + plasma system is minimized and effectively all microwave radiation from the source is ab-

sorbed. Given that with this impedance matching criterion, the physical positions of the metal stubs will depend on the impedance of the plasma Z_p (which partly affects Z_{in}), plasma properties can be derived from the fact that in the optimal system set-up the circuit is matched.

This paper describes a comparison between experiment and 3D electromagnetic models, where the waveguide geometry (including stub positions) is taken into account. In both model and experiment, minimisation of the reflection coefficient at the input port of the tuner + waveguide + plasma system is employed, which for the experiment is achieved via (auto-)tuning of the stub positions, while for the model this is achieved via tuning of the dielectric properties of the plasma (with given stub positions from experiment).

Three dimensional electromagnetic modelling of plasma reactors has been performed earlier, e.g. to find the geometry for optimal power transfer to the plasma [4] or to obtain the plasma impedance and plasma parameters [5]. An equivalent circuit method is being used by [5], which for a free-standing, inhomogeneous plasma is difficult. The dimensions of our reactor are such that an equivalent circuit approach is not as feasible as in [4]. Moreover, since our aim is to determine the reduced electric field, the equivalent circuit approach is insufficient. Obtaining plasma parameters from the plasma impedance Z_p, such as n_e and ν, as in [6], looks promising when combined with impedance matching, however, determining the plasma impedance in our geometry is not straightforward. Our approach is to perform 3D electromagnetic modelling, using commercial software ANSYS® [7], in which the the plasma is described as a parametrised dielectric medium. This medium is placed inside of the waveguide geometry, as it has been used in experiment. Subsequently, using the fact that the waveguide system is a matched circuit in experiment, parameters in the dielectric medium are scanned in order to result in the matching situation.

In this paper, first, details of the experimental setup are given with a discussion of discharge regimes encountered in the free-standing CO_2 microwave plasma. Additional experimental aspects of this work include the measurement of plasma dimensions, as well as electron density measurements obtained using microwave interferometry. The details of the model and approach are presented. Following this, results are presented regarding a CO_2 microwave plasma, from which plasma parameters are derived. Using neutral density values calculated using the pressure balance and the gas temperature, E/n_0 values are computed for different discharge regimes. After performing

the sensitivity analysis for both plasma and other materials, the next step is to use the best fitting parameter for $\gamma = \nu/\omega$, the normalised collision frequency (ω is the microwave angular frequency), to assess the electron temperature T_e, defined as 2/3 times the electron mean energy, providing a definition of temperature for a non-Maxwellian energy distribution. A validation of the methodology is performed using well-defined dielectric media, in both experiment and model, from which the expected accuracy of the approach is investigated. This validation is described in the appendix.

It is worth noting that the approach presented in this paper not only holds for CO_2 plasma, but for other types of plasma as well, also at other microwave frequencies (waveguide dimensions).

2 Experimental setup

2.1 Microwave plasma system

A schematic of the experimental and model setup is shown in figure 1. A 3-stub tuner [8] is connected to a microwave applicator, consisting of a waveguide of type WR-340 (width 86.36 mm, height 43.18 mm) with a quartz tube ($\varnothing_{in}$=27 mm, $\varnothing_{out}$=30 mm) penetrating perpendicularly through its wide walls. The quartz tube is bounded in several places by metal barriers, which at the bottom right of figure 1 is formed by the CO_2 gas injection system. In the experiment, gas is injected tangentially, leading to formation of a vortex flow which stabilises the ignited plasma in the center of the quartz tube [1], as indicated by the region with horizontal lines in figure 1. Microwaves from the source, with a frequency of 2.45 GHz, a wavelength λ_g and a characteristic (wave) impedance Z_0, enter the tuner + waveguide + plasma system from the left-hand side, which in the abscence of plasma would be reflected back on the 'short' on the right-hand side. The waveguide mode is TE_{10}, a transverse electric mode with the E-field perpendicular to the direction of propagation, and the H-field having components in the direction of propagation. Upon the ignition of plasma, the 3-stub tuner automatically matches the load impedance Z_L at the exit port of the tuner. The load reflection coefficient Γ_L is measured by the tuner system, from which the load impedance can be deferred. At the input port, Z_{in} is the impedance as seen into the tuner looking towards the plasma, with a corresponding reflection coefficient Γ_{in} at this interface for the microwave power incident

from the source. The short, or plunger, lays a distance $y = -\lambda_g/4$ away from the tube axis to align the anti-node of the standing wave with the center of the tube, to more easily ignite the plasma and maximise the power coupling.

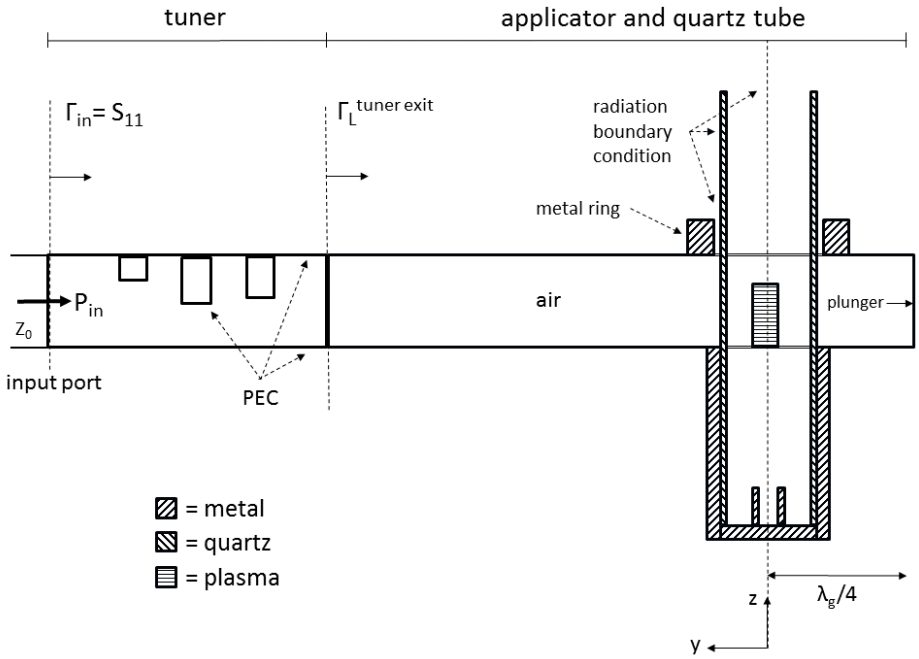

Figure 1: The reactor geometry with the 3-stub tuner and microwave applicator. The metal casing under the waveguide is the gas injection system, the metal ring on top is to prevent EM leakage from the waveguide. The boundary conditions for the corresponding numerical model are also indicated: PEC is a perfectly electric conducting boundary condition, while radiation boundary conditions are assigned at the quartz tube exterior and exit. Note that the axis is defined at the tube axis, so that the short is on the side of negative y.

2.2 Discharge regimes and measured plasma parameters

Depending on gas pressure p, mass flow rate $\dot{m}$, and microwave input power P_{in}, the plasma may exhibit two regimes: diffuse and contracted [9], see figure 2. The diffuse mode fills the quartz tube almost uniformly, while a

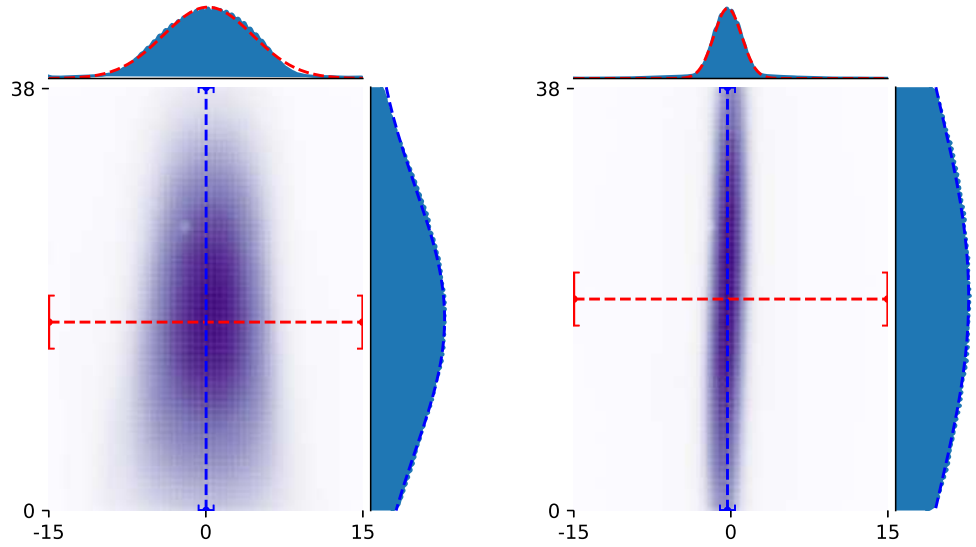

(a) (b)

Figure 2: Camera images of two types of plasma. The images are taken along the direction of the waveguide, i.e. looking in the direction of the generator. The spotted pattern is caused by the plunger grid. Also the Gaussian fits are shown, from which the plasma radial and axial widths are determined. (a) A diffuse plasma at 100 mbar, 3 slm, 800 W. (b) A contracted plasma at 250 mbar, 6 slm, 1400 W.

plasma in the contracted mode forms a thin filament. Since this leads to very different absorbed microwave power densities, up to a factor 15 higher in contracted versus diffuse, very different plasma properties can be expected between the two regimes. For a complete comparison, experiments and models are investigated in this work for both types of plasma. The conditions

for creating the diffuse and contracted CO_2 plasmas, as well as their apparent sizes, are given in table 1. Also estimates of the plasma volumes are given, that agree quite well with the respective power densities. Gas temperatures have been measured using Doppler broadening measurement of 777 nm triplet emission of atomic oxygen: 3500 ± 500 K for the diffuse plasma and 5500 ± 500 K for the contracted plasma, see figure 3. It can be seen that the gas profile can be regarded constant as a function of radial position in the plasma. Details of this technique can be found in [10, 11]. It has been

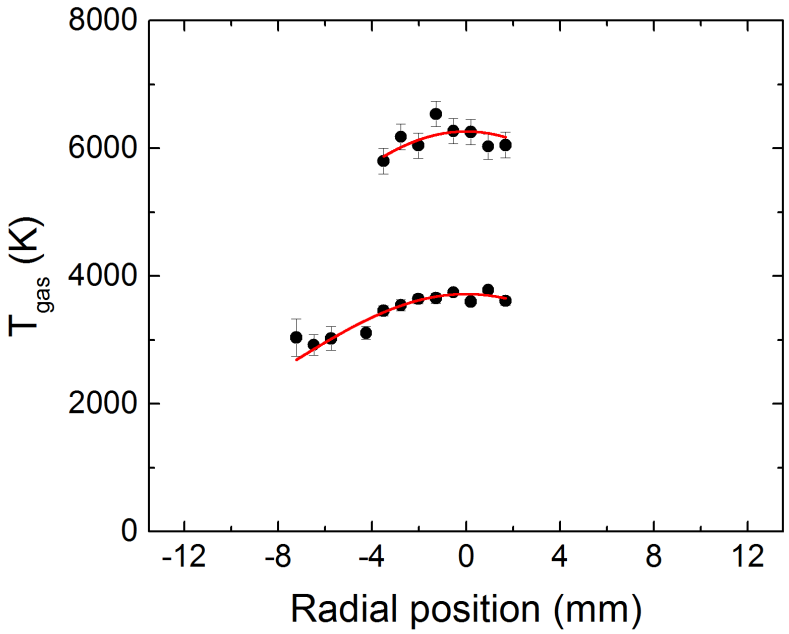

Figure 3: Gas temperature T_{gas} from Doppler broadened O atom 777 nm triplet of the diffuse and contracted CO_2 plasma, with respective Gaussian fits. The lower graph corresponds to the diffuse plasma, the upper graph to the contracted plasma. The diffuse plasma T_{gas} fit has a maximum of 3700 K, and a radial FWHM of 18 mm. The contracted plasma T_{gas} fit has a maximum of 6300 K, and a radial FWHM of 21 mm.

observed that these gas temperatures do not depend on the mass flow rate.

A Manta G145B digital camera is used to determine the optical emission profile of the plasma, as depicted in figure 2. For our cases, the camera

Table 1: Microwave input power P_{in}, gas pressure p and mass flow rate $\dot{m}$ for the two types of plasma studied. The values of the FWHM are determined from intensity profiles of atomic O emission, while the maximum electron density $n_{e,\text{max}}$ is determined from microwave interferometry measurements [11]. An estimate of the plasma volume is given.

	Diffuse plasma mode	Contracted plasma mode
P_{in} (W)	800 ± 10	1400 ± 10
$\dot{m}$ (slm)	3.0 ± 0.1	6.0 ± 0.1
p (mbar)	100 ± 5	250 ± 5
FWHM_r (mm)	10 ± 1	3.0 ± 0.1
FWHM_z (mm)	26 ± 3	35 ± 4
$n_{e,\text{max}}$ (m^{-3})	$(9.6 \pm 6.0) \times 10^{17}$	$(5.7 \pm 0.4) \times 10^{19}$
Plasma volume (m^3)	2×10^{-6}	3×10^{-7}

image collecting the total emission intensity is a very good indication of the emission of O, as can be seen in the supplementary information to this work. By using a bandpass filter of 777 ± 10 nm, predominantly the emission from atomic O is measured. These emission lines, which are directly populated from the electronic ground state via electron impact, has an intensity I_{777} which can be approximated as:

$$I_{777} \propto \frac{k_{\text{exc}}(T_e)\ [\text{O}]\ n_e}{\tau_{\text{rad}}\ k_Q\ n_0}\ , \tag{1}$$

where [O] is the ground state atomic oxygen density, n_e is the electron density, n_0 is the neutral particle density, $k_{\text{exc}}(T_e)$ is the electron impact excitation rate coefficient as a function of electron temperature, τ_{rad} the radiative lifetime of the excited O atoms and k_Q is the electronic quenching rate coefficient for excited atomic O due to collisions with heavy particles. More information on this technique can be found in the supplementary information. From equation 1 it can be seen that I_{777} is proportional to n_e. This proportionality is investigated further in the supplementary information. The neutral particle density n_0 is not constant over the plasma profile, since the gas temperature T_{gas} is not constant. The profile of the electron density n_e, however is assumed to be much steeper than that of T_{gas}, so that the gas composition is assumed to be constant over the n_e profile. For the contracted plasma, with its relatively high temperature, this even more holds for atomic oxygen, since the mole fraction of atomic oxygen hardly varies.

For the purpose of this work, the width of the 777 nm atomic O radial and axial emission profiles are considered equal to the width and height of

the n_e distribution in the plasma, to within an estimated accuracy of 10%, based on repeated measurements. The intensity profiles are approximated well by Gaussian distributions in both radial and axial directions, for which the Full Width Half Maxima (FWHM) are shown in table 1 for both pressure regimes.

Aside from the shape of the n_e distribution, line-integrated electron densities have been determined using the method of microwave interferometry [11]. This technique employs a microwave probe beam at a frequency of 140 GHz directed radially through the plasma. The phase shift incurred by the probe beam is a direct measure of the integrated electron density in the plasma, see [11] and [12] for further details. Using these measurements the absolute electron density profile is determined. The maximum values of the electron density, in the radial and axial center of the plasma, $n_{e,\max}$ have been calculated and are given in table 1. It can be seen that the contracted plasma has a much higher electron density at $n_{e,\max} = 5.7 \times 10^{19}$ m^{-3} compared to the diffuse plasma at $n_{e,\max} = 9.6 \times 10^{17}$ m^{-3}. Note, however, that the ionization degree always remains on the order of 10^{-5} to 10^{-4}, so that in all cases considered here the behavior of the plasma is controlled by electron-neutral interactions [11].

3 Model

The experimental geometry of figure 1 is implemented in ANSYS Electronics Desktop (ED), a Finite Element solver for Maxwell's equations. Using a set input power and frequency, the reflection coefficient is calculated for incident electromagnetic waves at the input port indicated in figure 1. In general an N-port network can be described by its impedances, or equivalently by a scattering matrix. The (complex) elements S_{ij} of the scattering matrix describe the ratio of the reflected wave amplitude coming from port i, and the incident wave amplitude driving port j [13]:

$$S_{ij} = \frac{V_i^{\text{refl}}}{V_j^{\text{in}}}. \tag{2}$$

For a shorted waveguide, as is the case here, the tuner and/or applicator have one port, so that the reflection coefficient Γ_{in} equals the (only) S-matrix element S_{11}, as indicated in figure 1. ANSYS ED directly calculates S_{11} at the input port. For the remainder of this paper, the reflection coefficient at

the input port (either from experiment or model) is referred to only as S_{11}. The impedance is perfectly matched when S_{11} goes to zero. In this case the impedance Z_{in} equals the characteristic impedance Z_0 of the waveguide. In order to estimate errors in the model, a validation with materials of varying conductivity has been preformed, see appendix A. For the plasma system, stub positions of the autotuner are transferred to the model. The plasma is implemented as a non-uniform dielectric medium, while the materials used for model validation are implemented using constant dielectric properties.

3.1 Plasma as a dielectric medium

In our experiments, a free-standing plasma is present inside a quartz tube crossing a waveguide applicator, see figure 1. Since plasma parameters, such as electron density, are non-uniform (see also figure 2), the assumption of a completely uniform plasma as made by e.g. Zakrzewski [6] is an oversimplification. Instead, the plasma is described by parametrising its dielectric properties based on a position-dependent electron density $n_e(r, z)$, and a constant effective electron-neutral collision frequency ν. In the supplementary information it is shown that γ can be considered constant within the electron density profile, when the T_{gas} profile is broader than the profile of the electron temperature T_e, which is plausible for the plasma cases considered. In the model, both $n_e(r, z)$ and ν are normalised using:

$$\eta(r, z) = n_e(r, z)/n_c \ , \tag{3}$$

$$\gamma = \nu/\omega, \tag{4}$$

where ω is the microwave angular frequency as stated earlier, and n_c the critical electron density (or cut-off density) given by:

$$n_c = \frac{\omega^2 \epsilon_0 m_e}{e^2}, \tag{5}$$

with ϵ_0 the permittivity of free space, m_e the electron mass, and e the electron charge, which is the density for which the electron plasma frequency is equal to the microwave angular frequency. This critical density n_c is 7.45×10^{16} m^{-3} for 2.45 GHz.

The complex relative permittivity [14] of the plasma can then be expressed in terms of η and γ as [4, 6]:

$$\text{Re}(\epsilon_p) \ = \ 1 - \frac{\eta(r, z)}{1 + \gamma^2} \ , \tag{6}$$

$$\mathrm{Im}(\epsilon_p) \;=\; -\;\frac{\eta(r,z)\;\gamma}{1+\gamma^2}. \tag{7}$$

Note that the conductivity σ of the plasma depends only on $\mathrm{Im}(\epsilon_p)$ via

$$\sigma = -\omega\epsilon_0 \mathrm{Im}(\epsilon_p). \tag{8}$$

Based on the I_{777} emission measurements (see equation 1), the spatial non-uniformity of the electron density is accounted for by using Gaussian profiles for $\eta(r,z)$:

$$\eta(r,z) = \eta_{\max}\,\exp(-r^2/(2\sigma_r^2))\,\exp(-(z-z_0)^2/(2\sigma_z^2)), \tag{9}$$

with σ_r and σ_z the distributions' standard deviations from which the radial and axial widths respectively are calculated, and z_0 the axial center of the plasma.

3.2 Modelling approach

For both the materials used in the validation system and the plasma, experimental conditions are replicated in the model. For the materials used for validation, where the dielectric properties are known a-priori and assumed to be accurate (see appendix), the goal is to test how accurately the reflection coefficient S_{11} measured in experiments can be replicated in the necessarily more simplified electromagnetic model. When using the autotuner in the microwave plasma system, minimum reflection coefficients are of the order of 0.01. The ultimate objective of the validation measurements is to determine whether such low reflection coefficients are easily reproduced in the modelled microwave system. Note that S_{11} concerns the amplitude reflection coefficient, meaning that the power reflection coefficient is the square of these values, making the latter significantly lower.

For the plasma, the goal is to vary either only γ, or γ and $\eta_{\max}$, or all four parameters γ, $\eta_{\max}$, σ_r and σ_z, until the reflection coefficient is minimised. As discussed in section 2.2, the parameters $\eta_{\max}$, σ_r and σ_z are, to a good approximation, known for the plasma conditions under consideration. Nonetheless, one of the aims of this work is to test the sensitivity of the reflection coefficient S_{11} to the dielectric material present in the waveguide.

A consistency check of the fitted normalised collision frequency γ is done by calculating γ for the diffuse and contracted case using NASA's CEA code

[15] and BOLSIG+ [16, 17] as a function of the reduced electric field. First, the equilibrium molar fractions of CO_2, CO, O and O_2 are calculated at T_{gas} between 3000 and 4000 K and between 5000 and 6000 K respectively. Molar fractions used for the diffuse case at 3500 K are 0.02629 (CO_2), 0.5185 (CO), 0.06327 (O_2), and 0.3920 (O). For the contracted case at 5500 K the molar fractions used are 0.004744 (CO_2), 0.4931 (CO), 0.0004160 (O_2), and 0.5017 (O). Subsequently, the collision frequency ν is calculated for a reduced electric field range. The collision frequency $\nu = \gamma\omega$ is related to the electron energy distribution function (EEDF) f as:

$$\nu = \sum_{i=1}^{\text{species}} \nu_i = \sum_{i=1}^{\text{species}} n_{0,i} \int_0^\infty f(\mathcal{E}) \sigma_{\text{tot},i}(\mathcal{E}, T_{\text{gas}}) \mathcal{E} \sqrt{\frac{2}{m_e}} d\mathcal{E}, \tag{10}$$

where $n_{0,i}$ is the neutral gas density of species i, $\sigma_{\text{tot,i}}$ the total cross section for electron-neutral collisions with species i, and $\mathcal{E}$ the electron energy. The cross section σ_{tot} will depend on the composition of the gas, which to a good approximation depends only on T_{gas} for the high temperatures present in the plasma.

Since the output of the electromagnetic model directly provides the E-field distribution within the plasma, the reduced electric field E/n_0 is easily obtained. This value of E/n_0 is also compared with the one resulting from the CEA/BOLSIG+ code. The cross sections from lxcat [18] that have been used, are from the Phelps database [19–22] (CO_2, CO and O_2), and of Blaha [23] (for atomic O). For a thorough discussion on using cross sections for modelling CO_2 conversion, see for example [24].

4 Results and discussion

4.1 Plasma

The values for η_{max} obtained with microwave interferometry are $\eta_{\text{max}} = 13 \pm 8$ for the diffuse plasma, and $\eta_{\text{max}} = 765 \pm 54$ for the contracted plasma (deduced from the values in table 1). The fitting approaches in which all parameters have been fit (i.e. η_{max}, γ, FWHM_r and FWHM_z) and for which only η_{max} and γ have been fit, lead to good impedance matching ($|S_{11}^{\text{sim}}|$ of the order of 0.01). The resulting values of either η_{max} or the plasma width, however, do not agree with the experimental values. See table 2 for an overview of these results. In this approach it is not straightforward to assign an uncertainty

Table 2: Modelling results for varying $\eta_{\max}$, γ and/or width. The corresponding values of $|S_{11}|$ are of the order of 0.01, except for $\eta_{\max} = 680$ (contracted) for which $|S_{11}| = 0.001$. The parameter values, however, do not agree with the values found with independent measurements.

Plasma mode	$\eta_{\max}$	FWHM$_r$ (mm)	FWHM$_z$ (mm)	γ
Diffuse	15	15	13	2
	35	10	18	4
	48	10	18	5
	90	10	26	14
Contracted	224	3.0	35	0.8
	500	2	42	1.0
	680	2.0	80	1.4
	2220	1.5	52	1.5

to these parameter values, since the values merely have adapted to absorb maximum input microwave power, but without any direct reference values. The solution of the diffuse plasma with $\eta_{\max} = 15$ even has a radial width that is larger than the axial width. For the contracted plasma, fitting all parameters resulted in $\eta_{\max} = 680$, which deviates 11% from the measured electron density, with excellent matching ($|S_{11}| = 0.001$). For $\eta_{\max} = 680$ the resulting γ, FWHM$_r$ and FWHM$_z$ are 1.4, 2 mm and 80 mm respectively, see also table 2. These widths deviate too much from experiment. At given stub positions, the measured plasma width is a rather strict condition, since the plasma shape is such that it absorbs the microwave power efficiently. Assigning the measured width in the two plasma cases, but varying both $\eta_{\max}$ and γ, also does not lead to an agreement of the electron density with measured values. This shows that, while fitting for all parameters does provide solutions, it does not necessarily lead to a solution that results in parameters which compare well with independent measurements.

Constraining the degrees of freedom in the fitting procedure is necessary, because of (i) the high sensitivity of S_{11} to the input parameters, and (ii) the systematic deviations between model and experiment, as discussed in the appendix, since all parameters except γ are known from independent other measurements.

Fitting γ only, and keeping the experimental values of $\eta_{\max}$ and the plasma widths fixed, leads to reasonable impedance matching: $|S_{11}^{\text{sim}}| = 0.20$ for the diffuse plasma, and $|S_{11}^{\text{sim}}| = 0.25$ for the contracted plasma. Figure 4 shows

$|S_{11}|$ as function of γ near the minimum for both plasma conditions. The function is plotted for the measured $\eta_{\max}$ as well as for the values based on the uncertainty in the measurement of n_e (see table 1). Since this uncertainty is larger for the diffuse plasma, the behaviour for the different values of $\eta_{\max}$ is more distinct than for the contracted case. In the diffuse plasma case, $|S_{11}|$ reaches 0.1 for the upper limit of the measured $\eta_{\max}$, which shows that better matching is feasible within the error in the measurement. This is not the case for the contracted plasma, for which the uncertainty range in $\eta_{\max}$ is smaller. The estimation of the width of the plasma however, is perhaps not good enough: in the contracted plasma case, the sensitivity to the width is higher, because of the larger electron density. Error bars indicate the uncertainty in $|S_{11}|$ due to an assumed 10% uncertainty in the measured $\eta_{\max}$. Although the experimental uncertainty is higher for the diffuse plasma case, we assume $\eta_{\max}$ to take the nominal measured value. This nominal value has been set in the model. Assuming an absolute error $|\Delta S_{11}| < 0.1$ around the minimum, this uncertainty leads to a range of $1.6 < \gamma < 3.2$ for the diffuse plasma, and $1.3 < \gamma < 5.7$ for the contracted plasma. In the model, $|S_{11}|$ depends weakly on a spatial variation of γ, so that the model is consistent with the assumption that γ is spatially constant. The conductivity σ is calculated using the ranges of $\eta_{\max}$ and γ in equation 8. For the diffuse plasma 0.2 S/m $< \sigma <$ 1.3 S/m, for the contracted plasma 20 S/m $< \sigma <$ 60 S/m. The diffuse plasma conductivity corresponding to the upper limit of $\eta_{\max}$ is of the order of 1 S/m, which is more reliable than for the lower limit according to the validation with NaCl solutions (see appendix). The contracted plasma conductivity is an order of magnitude higher, which is outside the regimes investigated in the validation, but validation using copper indicates that the model is still accurate to within 10% for highly conducting media.

The modelled electric field for both plasma cases, at the measured $\eta_{\max}$ and FWHMs, and at γ=2.4 and 3.4 respectively (corresponding to the minima in fig. 4), are given in figures 5 and 6. In both cases the electric field peak values have a similar order of magnitude (10^4 V/m), but the distribution is clearly different. Because of the larger skin depth (the distance over which the electric field strength in a material decreases by a factor of $1/e$) in the diffuse case, the electric field decreases only slightly, while in the contracted case it falls off more steeply.

The reduced electric field E/n_0 is calculated with E from the model and the neutral gas density n_0, which is calculated using the ideal gas law for the experimental T_{gas} values 3500 $\pm$ 500 K (diffuse plasma) and 5500 $\pm$ 500 K

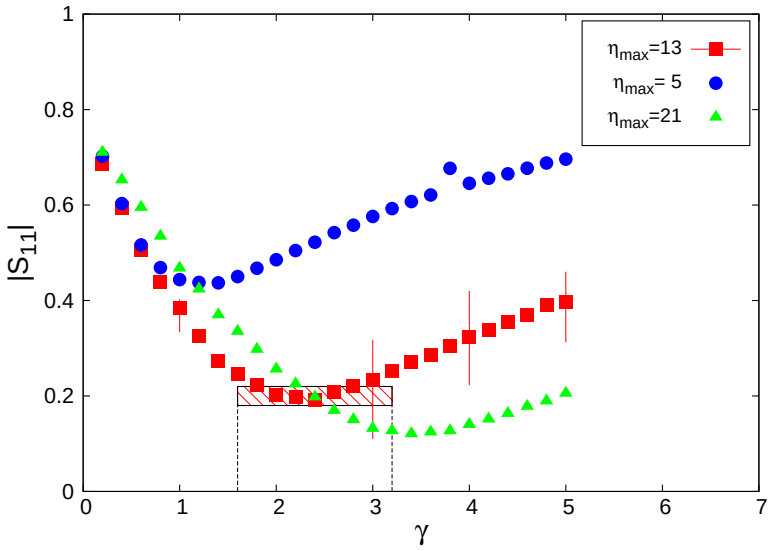

(a)

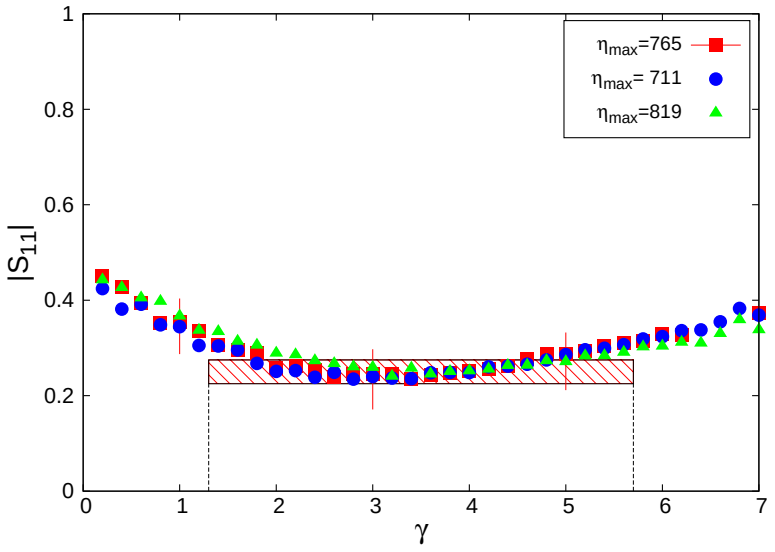

(b)

Figure 4: $|S_{11}|$ as function of γ for the measured values of $\eta_{\max}$, FWHM$_r$ and FWHM$_z$. Also $|S_{11}|$ is shown for the values of $\eta_{\max}$ which are the bounds of the uncertainty in the measurement. The shaded box shows the uncertainty in γ based on a 10% uncertainty in $|S_{11}|$. Also the uncertainty due to a 10% uncertainty in $\eta_{\max}$ is shown for a few values of γ. (a) Diffuse plasma. (b) Contracted plasma.

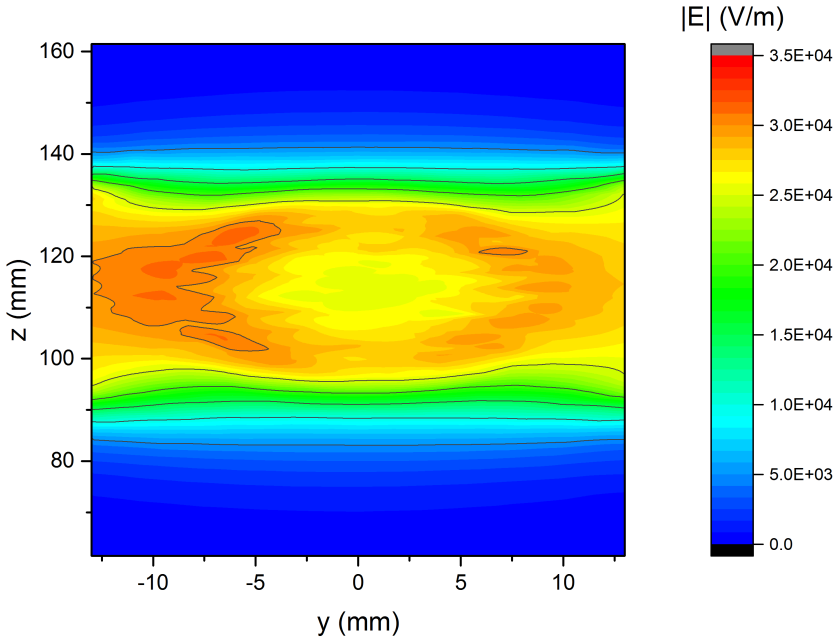

Figure 5: The electric field of the diffuse plasma, $\mathrm{FWHM}_r = 10$ mm, $\mathrm{FWHM}_z = 26$ mm, $\eta_{\max} = 13$, and $\gamma = 2.4$. A vertical slice through the plasma cylinder is shown in the plane of figure 1 and perpendicular to figure 2. The direction of y is along the full quartz tube width. The field is only slightly lower in the center due to the relatively large skin depth.

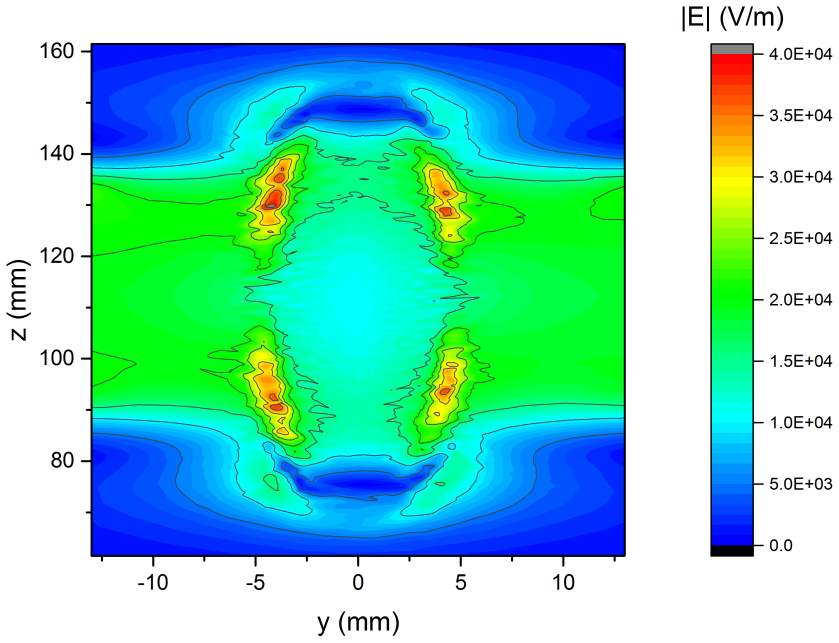

Figure 6: The electric field of the contracted plasma, $\mathrm{FWHM}_r = 3$ mm, $\mathrm{FWHM}_z = 35$ mm, $\eta_{\max} = 765$, and $\gamma = 3.4$. A vertical slice through the plasma cylinder is shown in the plane of figure 1 and perpendicular to figure 2. The direction of y is along the full quartz tube width. The field is significantly lower in the center, because of the skin effect.

Table 3: Modelling results for measured $\eta_{\max}$ and width, and varying γ. The corresponding values of $|S_{11}|$ are of the order of 0.1.

Plasma mode	$\eta_{\max}$	FWHM$_r$ (mm)	FWHM$_z$ (mm)	γ
Diffuse	13	10	26	$1.6 < \gamma < 2.3$
Contracted	765	3	35	$2 < \gamma < 3$

(contracted plasma). In the center of the plasma this leads to ranges of E/n_0 of 80 to 180 Td for the diffuse plasma, and 10 to 60 Td for the contracted plasma, based on 10% uncertainty in $|S_{11}|$. An error estimate of the reduced electric field at the center, based on the error in the gas temperature alone, leads to 120 ± 20 Td for the diffuse plasma and 30 ± 3 Td for the contracted plasma, which is smaller than the uncertainty in the numerical model.

As a consistency check, the modelled values of γ and E/n_0 are compared with calculations performed using CEA for the molar fractions of the gas composition, and BOLSIG+ for calculating γ. Figure 7 shows γ vs. E/n_0 [18, 20–23], and the shaded boxes show the γ- and E/n_0-ranges from the model. To investigate the effect of gas composition on γ vs E/n_0 the γ values for pure CO_2 at 3500 K (diffuse) and 5500 K (contracted) have been calculated using BOLSIG+ [18]. In both plasma cases, γ is sensitive to the thermal equilibrium composition in the model's reduced field range. Therefore, knowledge of the plasma gas composition at a given temperature, gives insight to the value of γ.

Using the modelled E/n_0, the calculated values of γ for the indicated temperature range lie well within the range of γ as determined from the EM model. The higher range of γ found from the model is clearly overestimated, especially in the contracted case. Knowing the measured T_{gas} and having the E/n_0 from the model, the estimated γ range can be narrowed down. From figure 7 it can be seen that with T_{gas} the range determined by the shaded box can be reduced to the range indicated by the dashed lines. The result is $1.6 < \gamma < 2.3$ for the diffuse plasma, and $2 < \gamma < 3$ for the contracted plasma. So, the model is able to calculate γ and E/n_0 quite well, and leads to physically plausible values.

The reduced electric field throughout the plasma is clearly spatially distributed according to the electric field strength and T_{gas}. Figure 8 shows the (reduced) electric field along the tube diameter through the center of the plasma, instead of only at the center. The gas temperature profile is measured between -5 and 5 mm along the tube diameter. Gaussian fits of the

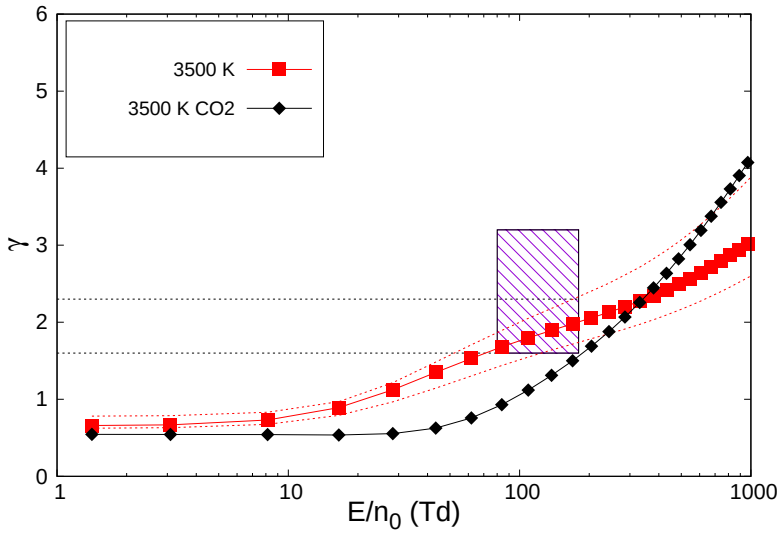

(a)

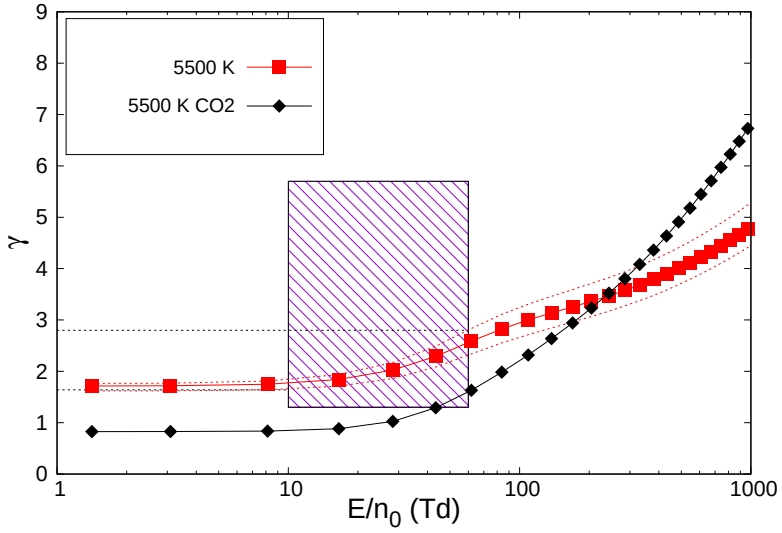

(b)

Figure 7: Normalised collision frequency γ vs. reduced electric field. These are obtained from BOLSIG+ (molar fractions from CEA). The boxes show the ranges of γ and E/n_0 from the electromagnetic model. Using the measured T_{gas} for these plasma cases, the γ range is narrowed down from the vertical range of the box to the horizontal dashed lines. Also γ is shown for pure CO_2 at the nominal value. (a) Diffuse plasma. (b) Contracted plasma.

radial T_{gas} data show that the FWHMs are 18.3 and 21.4 mm, making T_{gas} nearly flat in the plasma region. This also holds for the n_0 profile, and that means that the shape of the reduced electric field directly follows the shape of the electric field.

The direct relationship between T_e and E/n_0 [25] provides an extra check on the internal consistency of the methodology used in this work. Having the ranges of γ and the reduced electric field established, an estimate is made of the electron temperature T_e. Figure 9 shows BOLSIG+ calculations of the electron temperature T_e (in eV) versus the reduced electric field of the thermal equilibrium composition. For the diffuse plasma, based on a reduced electric field range of 80 to 180 Td, 2 eV $< T_e <$ 3 eV, and for the contracted plasma (10 to 60 Td), 0.5 eV $< T_e <$ 1 eV. The lower value of T_e in the contracted regime is consistent with the decreasing T_e that tends towards T_{gas} for increasing pressure [3]. The reported value of T_e also agrees with [9].

It has to be mentioned that, although in BOLSIG+ the superelastic collisions as well as electron-electron collisions were enabled, this is still a too simple approach. We merely used BOLSIG+ to illustrate how the γ-range can be narrowed down, and how an estimate can be made of T_e. It is known that more complete models exist, taking into account superelastic vibrational and electronical collisions, and the influence on plasma composition, e.g. see reference [26]. A more careful study using this approach takes into account the influence on the EEDF, not only of CO_2 [27], but also CO [28], which has a substantial molar fraction at these high temperatures. Since we have performed our calculations assuming thermal equilibrium compositions, an estimate has to be made of how good this assumption is, i.e. how does thermal dissociation compete with electronically induced dissociation. The rates of electron impact dissociation and dissociative recombination at the temperatures and pressures in this paper are comparable to rates for thermal dissociation, mainly due to the large cross section of dissociation of CO. Also, the degrees of ionisation of both the diffuse (10^{-5}) and the contracted (10^{-4}) plasma are relatively high, and therefore letting the plasma (electron) rates compete with the thermal dissociation rates and changing the composition [26]. Therefore the narrowing down of the γ-range and the estimate of T_e can be improved using the more complex models mentioned in [26–28]. Since the superelastic collisions have the effect of enlarging the EEDF in the tail (and be smoothened by electron-electron collisions) [27], the BOLSIG+ EEDFs are possibly underestimated. The value of γ (at fixed gas temperature) however is quite insensitive to changes in the EEDF, but could be affected at

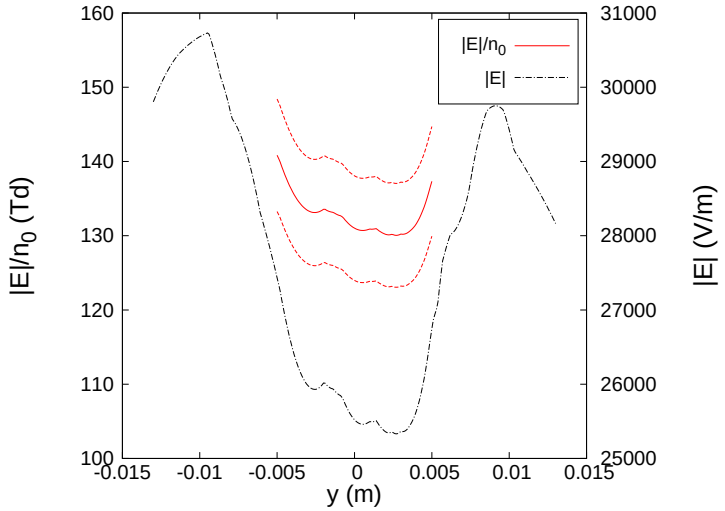

(a)

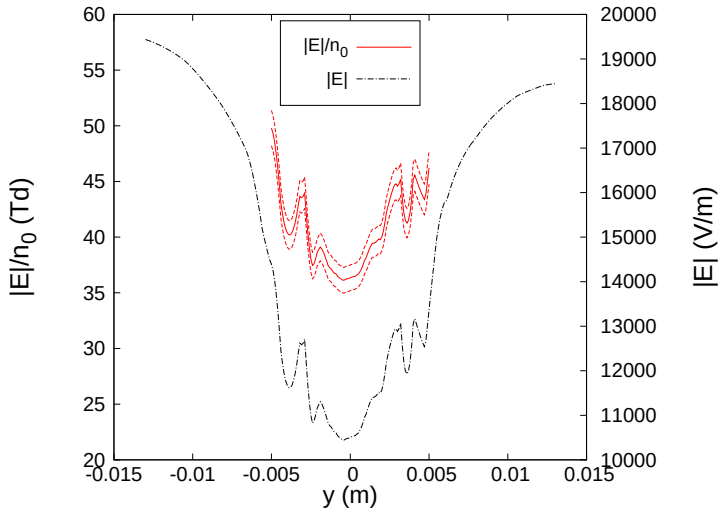

(b)

Figure 8: The reduced electric field along the tube diameter for the diffuse and contracted plasmas with conditions as in figures 5 and 6 respectively. The neutral density profile used, is based on experiment. The direction of y is along the quartz tube diameter, where negative y is at the side of the short. The $|E|/n_0$ is given for an n_0 profile from experiment and modelling. The electric field from the model is given over the full tube diameter. (a) Diffuse plasma. (b) Contracted plasma.

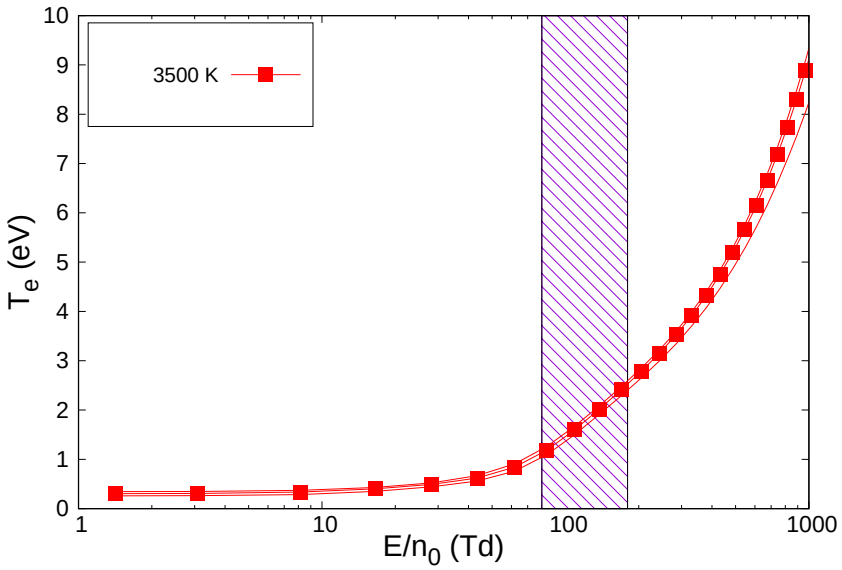

(a)

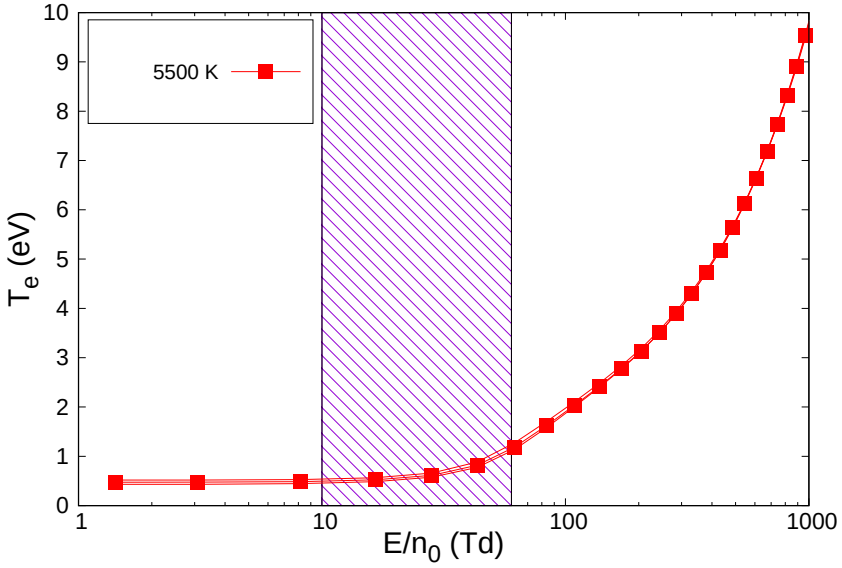

(b)

Figure 9: Electron temperature T_e vs. reduced electric field. These are obtained from BOLSIG+ (molar fractions from CEA). The boxes show the ranges E/n_0 from the electromagnetic model. (a) Diffuse plasma. (b) Contracted plasma.

lower E/n_0 values. This could therefore affect mainly the results of the contracted plasma case. Especially for lower E/n_0 values, this could mean that γ is underestimated. The same would hold for average electron energy, i.e. due to underestimation of the EEDF, also the average electron energy could be underestimated.

5 Conclusions and outlook

It has been shown that it is possible to determine the reduced electric field E/n_0 of a free-standing CO_2 microwave plasma, using 3D electromagnetic modelling with the principle of impedance matching. The plasma has been described as a dielectric medium only. One of the difficulties in modelling such a free-standing plasma is the presence of systematic errors, e.g. the position of the dielectric, and power leakage. Another difficulty is the high sensitivity to all input parameters, so that a procedure based on fitting all parameters at once (i.e. $\eta_{\max}$, γ, and $\mathrm{FWHM}_{r,z}$) leads to solutions not in agreement with independent measurements of the parameters determined. Therefore a procedure has been performed, fitting only the normalised collision frequency γ and using experimental input for the remaining parameters. The reduced electric field of the diffuse plasma (p=100 mbar, P=800 W, T_{gas}=3500 $\pm$ 500 K) lies between 80 and 180 Td, for the contracted plasma (p=250 mbar, P=1400 W, T_{gas}=5500 $\pm$ 500 K) it lies between 10 and 60 Td. For the diffuse plasma γ lies between 1.6 and 2.3, and for the contracted plasma between 2 and 3. Although there is an uncertainty in the range of γ, the combination with the resulting reduced electric field range fits very well in the results based on calculations made with CEA/BOLSIG+ for a CO_2 microwave plasma. Moreover, it is has also been shown that, based on these results, an estimate can be made of the electron temperature. For the diffuse plasma T_e lies between 2 and 3 eV, for the contracted plasma T_e lies between 0.5 and 1 eV. Using CEA/BOLSIG+ with the given cross sections, however, leaves out the effects of superelastic vibrational en electronic collisions, so that our results probably underestimate the values of γ and T_e for the lower $\mathrm{E/n_0}$. Better results in narrowing down the γ range, and estimating T_e may be obtained by exploring the usage of more complex models, e.g. [26–28].

It is clear that the method described in this paper is not very easy to apply, and it would therefore be both interesting and helpful to apply this method to plasma systems that are more standard, like a surface wave dis-

charge, see for example [29].

In this paper γ has been found for known n_e. When, on the other hand, γ is known from experiment, the method described in this paper can be used to find n_e in a similar way.

6 Acknowledgements

This work is part of the TKI HTSM Solid State Plasma project, and the Plasma Power to Gas research programme with project number 13581, which is co-financed by the Netherlands Organisation for Scientific Research (NWO) and Alliander N.V.

The work of F.J.J. Peeters is part of project EnOp of the Interreg V programme Flanders-Netherlands, with financial support from the European Union.

We would like to thank M. Parente of DIFFER for preparing the NaCl solutions.

7 Supporting Information Available

S1 contains information on the I_{777} intensity and the deferred electron density profile.

S2 explains the assumption of constant γ in the plasma.

References

[1] W. Bongers, H. Bouwmeester, B. Wolf, F. Peeters, S. Welzel, D. van den Bekerom, N. den Harder, A. Goede, M. Graswinckel, P.W. Groen, J. Kopecki, M. Leins, G. van Rooij, A. Schulz, M. Walker and R. van de Sanden, Plasma Processes Polym., 2017, 14, e1600126.

[2] R. Snoeckx and A. Bogaerts, Plasma technology - a novel solution for CO_2 conversion?, Chem. Soc. Rev., 2017, 46, 5805.

[3] A. Fridman, Plasma Chemistry, Cambridge University Press, 2008.

[4] H. Nowakowska, M. Jasinski, P.S. Debicky and J. Mizeraczyk, Numerical Analysis and Optimization of Power Coupling Efficiency in Waveguide-Based Microwave Plasma Source, IEEE Transactions on Plasma Science, Vol. 39, NO. 10 October 2011, p. 1935.

[5] M. Shuto, H. Ohmi, H. Kakiuchi, T. Yamada and K. Yasutake, Determination of plasma impedance of microwave plasma system by electric field simulation, J. Appl. Phys. 122, 043303 (2017).

[6] Z. Zakrzewski, Bull. Acad. Polonaises des Sci., Série Sci. et Tech. Vol. XIV, 939, 1966.

[7] ANSYS® Electronics Desktop™ 2015.2.0 and its documentation.

[8] Homer Hot Measurement and Tuning System, User's Handbook, S-TEAM Lab.

[9] N. den Harder et al, Homogeneous CO_2 conversion by microwave plasma: Wave propagation and diagnostics, Plasma Processes and Polymers 2016, DOI 10.1002/ppap.201600120.

[10] A. E. Shumack, V. P. Veremiyenko, D. C. Schram, H. J. de Blank, W. J. Goedheer, H. J. van der Meiden, W. A. J. Vijvers, J. Westerhout, N. J. Lopes Cardozo and G. J. van Rooij, Phys. Rev. E 78, 046405 (2008).

[11] A.J. Wolf et al, The relationship between discharge contraction and electron density in radially confined CO_2 microwave discharges. To be published.

[12] A.V. Golubev, E.G. Krasheninnikov, and E.A. Tischchenko, Electron Density and Effective Collision Frequency Measurements in CO_2 UHF-Discharge by Microwave Diagnostic Techniques, ICPIG 15, P-1718, 1981.

[13] D.M. Pozar, *Microwave Engineering*, Fourth Edition, John Wiley and Sons, 2012.

[14] M.A. Lieberman, A.J. Lichtenberg, Principles of Plasma Discharges and Materials Processing, John Wiley and Sons, 1994.

[15] NASA Chemical Equilibrium with Applications, https://www.grc.nasa.gov/WWW/CEAWeb/, last updated 02/04/2016.

[16] G.J.M. Hagelaar and L.C. Pitchford, Solving the Boltzmann equation to obtain electron transport coefficients and rate coefficients for fluid models, Plasma Sources Science and Technology 14, 722, 2005.

[17] BOLSIG+ version 03-2016.

[18] Phelps database, www.lxcat.net, retrieved on March 22, 2019.

[19] R.D. Hake, Jr. and A.V. Phelps, Phys. Rev. 158, 70 (1967).

[20] Phelps database, CO_2 cross sections.

[21] Phelps database, CO cross sections.

[22] Phelps database, O_2 cross sections.

[23] M. Blaha and J. Davis, Phys. Rev. A 12, 2319 (1975).

[24] A. Bogaerts, W. Wang, A. Berthelot and V. Guerra, 2016 Plasma Sources Sci. Technol. 25 055016.

[25] G.J.M. Hagelaar, K. Hassouni, A. Gicquel, Interaction between the electromagnetic fields and the plasma in a microwave plasma reactor, Journal of Applied Physics 96, 1819, 2004.

[26] M. Capitelli, G. Colonna, G. D'Ammando and L.D. Pietanza, 2017 Plasma Sources Sci. Technol. 26 055009.

[27] L.D. Pietanza, G. Colonna, G. D'Ammando, A. Laricchiuta, and M. Capitelli, Physics of Plasmas 23, 013515 (2016).

[28] L.D. Pietanza, G. Colonna and M. Capitelli, 2017 Plasma Sources Sci. Technol. 26 125007.

[29] G.M. Petrov, J.P. Matte, I Pérès, J. Margot, T. Sadi, J. Hubert, K.C. Tran, L.L Alves, J. Loureiro, C.M. Feireira, V. Guerra, and G. Gousset, Plasma Chemistry and Plasma Processing, Vol. 20, No. 2, 2000.

[30] Agilent PNA E8362B Network Analyzer.

[31] Borosilicate Glass, Goodfellow Ceramics and Glass Division, http://www.goodfellow-ceramics.com, downloaded 14/02/2018.

[32] Conductivity Sensor BT27i User's Guide, Centre for Microcomputer Applications, http://www.cma-science.nl, downloaded 19/02/2018.

Appendix

A Model validation

A.1 Microwave system

For validation of our approach, experiments have been performed on a set of dielectric or conducting materials, placed in the waveguide at the position of the quartz tube and plasma. Instead of using the microwave source and autotuner employed in the microwave plasma system, the applicator waveguide is connected to a network analyser (PNA [30]). Insulating, conducting and highly conducting materials have been chosen to investigate: teflon (rod, conductivity $\sigma \approx 1 \times 10^{-4}$ S/m), NaCl solutions (of different concentrations, in a glass cylinder), and copper (rod, $\sigma \approx 6 \times 10^{7}$ S/m) respectively. Teflon and copper in the model are taken from the ANSYS material's database, the model's properties for the glass cylinder are taken from [31]. The NaCl solutions have conductivities of 0.01, 0.1 and 1.0 S/m. The conductivities are based on suggested calibration solutions for the BT27i conductivity sensor [32], that we also assume to be accurate. The accuracy of the solutions is high. Deviations due to changes in the lab temperature are assumed to be negligible.

The solutions have also been translated with respect to the tube axis: 3 mm towards the PNA sender/receiver and 3 mm towards the short. Reflection coefficients and impedances are measured for a frequency sweep from 2.0 to 3.0 GHz. No tuning is performed in these measurements, i.e. the reflection coefficients are not minimised and measured as is. The reflection coefficient simply takes the value resulting from reflection of the forward propagating microwaves on the materials and short at the end of the waveguide. For the model validation system, reflection coefficients are calculated over a frequency range of 2.0 to 3.0 GHz in steps of 0.01 GHz. The focus is on 2.41 to 2.49 GHz, since the frequency of interest is 2.45 GHz. As a check, two different boundary conditions are compared in the model of the NaCl solu-

tion with the highest conductivity (1 S/m): (i) a radiation (or absorbing) boundary condition [7] directly on the cylinder, and (ii) an 'air box' placed around the reactor geometry of figure 1, with its faces assigned a radiation boundary condition.

Apart from lossy dielectrics and radiation boundaries the model is assumed lossless.

A.2 Results

We define the error between the measured and modelled (complex) reflection coefficients at the microwave frequency of interest, 2.45 GHz, as $\Delta S_{11} = S_{11}^{\text{exp}} - S_{11}^{\text{sim}}$. For the poorly conducting teflon its absolute value $|\Delta S_{11}| = 0.06$, while for the highly conducting copper $|\Delta S_{11}| = 0.1$. The NaCl solutions are conducting media that are electrically similar to a plasma. Figure 10 shows ΔS_{11} for the NaCl solutions. The notation ΔS_{11} is also used in this figure for the difference in the experimental values of S_{11} between moving the NaCl solutions 3 mm away (towards the PNA receiver) and towards the short. A scan of more positions in the validation set up is not feasible, because of the limited space between the glass cylinder and the hole in the waveguide. The experimental uncertainty in position, however is only 1 mm, so assuming linear behaviour, the uncertainty in position of the dielectric medium can result in a $|\Delta S_{11}|$ of about 0.1. At 2.45 GHz, the difference in S_{11} between the off-axis and on-axis positions is mainly due to the change of phase of both the real and imaginary part. Since $\text{Re}(S_{11})$ as a function of frequency is on the rising edge at 2.45 GHz, and $\text{Im}(S_{11})$ is on the falling edge, both are sensitive to the phase change. The overall behaviour of S_{11} is very similar at each conductivity. The difference in $|S_{11}|$ between using the two different boundary conditions in the model, i.e. either the air box or the radiation boundary condition, is not higher than 0.02 (not shown in the figure). Therefore, using either boundary condition is reliable within the 0.1 uncertainty in $|S_{11}|$. All systematic errors therefore lead to an estimated absolute error in S_{11} of about 0.1 between model and experiment.

It is possible that a portion of the input power that is not absorbed by a dielectric medium (such as a plasma), leaks from the reactor, e.g. via radiation through small holes or due to non-perfectly conducting walls. At the microwave input side, this leads to a somewhat lower reflected input power, so a lower $|S_{11}|$, which may be misinterpreted as absorption by the dielectric medium. The numerical model takes some of this power leakage into

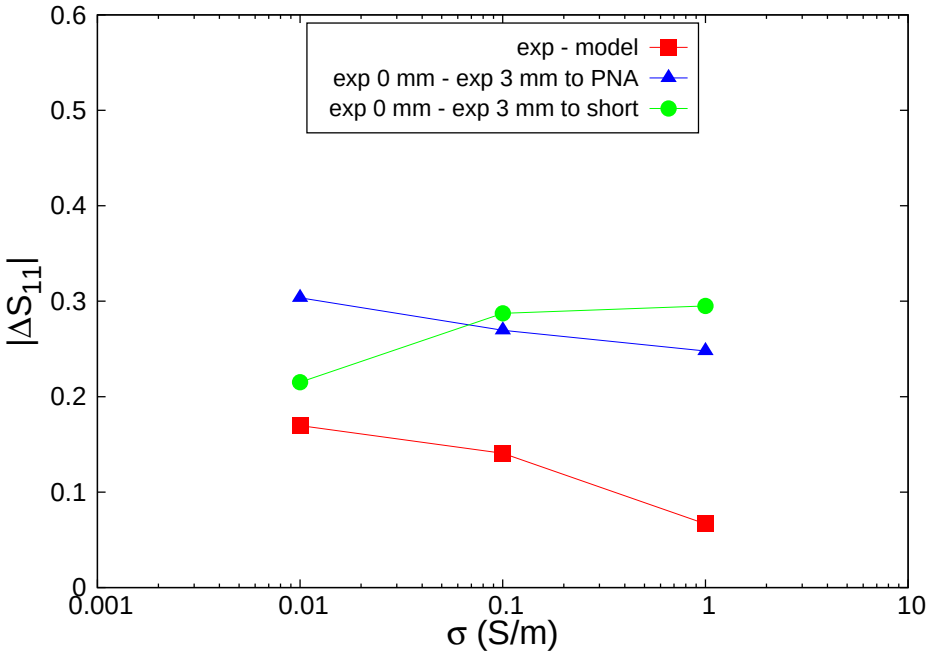

Figure 10: Error in reflection coefficient ΔS_{11} for NaCl solutions of different conductivity. The conductivities are based on prescribed calibration solutions. Two types of error are shown: the difference in $|S_{11}|$ between model and experiment (squares), and the difference in $|S_{11}|$ between two positions of the glass cylinder in experiment only (towards the PNA receiver (triangles) and towards the short w.r.t to the tube axis (circles)).

account via radiation boundary conditions, but the walls of the waveguide in the model are regarded perfectly conducting. The power leakage due to walls of finite conductivity is assumed to be small.

The case with the NaCl solution of 1 S/m has the smallest error, $|\Delta S_{11}| = 0.07$, so that plasmas of a conductivity of that order are best described by the model.